Dynamics and Control of a Large Space Antenna

Shyh Jong Wang* and Jonathan M. Cameron†
California Institute of Technology, Jet Propulsion Laboratory, Pasadena, California

Large space antennae will play an important role in space utilization in the coming decades. In this paper, a control design study of a large space-deployable antenna is presented. For comparative analysis, three controller-estimators were designed and optimized based on requirements of focused communications missions, disturbances, and hardware configurations. One of the major issues investigated is the effect of model error sensitivity. Stability margins, surface accuracy, and pointing errors have been obtained over a wide range of model parameter variations. The results show that structural uncertainties and model errors can cause serious control deterioration. Performance can be improved by strengthening certain structural elements. Flight experiments and in-flight system identification are imperative measures for reducing mission risk and enhancing performance.

I. Introduction

LARGE space antennae and other large space structures will play an important role in the coming decades as commercial applications of space become feasible, especially in the area of communications. Structures of 10-120 m and larger have been considered by NASA and other government agencies for future missions.[1] As the structural size and mass distribution change drastically from those of conventional spacecraft, many difficult control problems arise. The basic problem, however, comes in modeling highly flexible structures. Structures of this type are known to have a large number of packed modes at very low frequencies. Mode shapes and frequencies cannot be accurately predicted or measured for even a small number of modes at preflight time. This means model uncertainties. Model uncertainties in the control loop can cause serious consequences, including the possibility of making the system unstable. Model order is another problem having great impact on control design. Using today's in-flight computer capability, one can expect to have only a modest-order controller—which often means model truncation and which will further performance deterioration. Dynamics and control problems for specific configurations must be characterized and evaluated in terms of incomplete knowledge of the system dynamics so that the required performance can be insured and the risk reduced.

In this paper, the structural dynamics and the control properties for a 64-m-diam mesh deployable antenna are investigated. Some interesting results are presented on the effects of model parameter uncertainties to the system stability, surface accuracy, and pointing accuracy. Critical control problems are identified and potential solutions recommended. In Sec. II the antenna configuration and the structural dynamic properties are briefly described. The control design, disturbance assessment, hardware sizing, and construction of weighting matrices are summarized in Sec. III. Numerical results are presented in Sec. IV and control design issues relevant to rf (radio frequency) beam pointing in Sec. V. Conclusions are drawn in Sec. VI.

Presented as Paper 82-1568 at the AIAA Guidance and Control Conference, San Diego, Calif., Aug. 9-11, 1982; submitted Aug. 27, 1982; revision received March 16, 1983.

*Member of Technical Staff, Control and Energy Conversion Division. Member AIAA.

†Engineer, Control and Energy Conversion Division. Member AIAA.

II. The Antenna Configuration and Structural Dynamic Properties

A. Antenna Configuration

Several communications antenna concepts are under development.[1-3] The antenna chosen for analysis is a pretensioned mesh deployable structure. Figure 1 shows the major components of a 122-m-diam point design antenna. The basic structural components are the feed assemblies, mast, hoop, and reflector mesh surface. The mast and support cables suspend the hoop and together the assembly provides the stiffness of the structure. The mesh is suspended by the hoop and the mast. The surface shape is controlled by the shaping cables through a secondary draw surface and tie cords. The cables are made of stranded quartz cords. The hoop consists of 48 graphite fiber hollow sections. The adjacent sections are joined together through hinges. The reflector is made of gold-plated poly-wire mesh. The four circular surface areas are separately illuminated by the feed elements that form the offset feed quad aperture arrangement.

B. Structural Dynamic Properties

To assess performance, a finite element model of a 64-m-diam antenna has been adopted. The reflector and the hoop were modeled by a two-for-one model with 24 gore and hoop sections and 120 grid points. The feeds, solar panels, mast, etc., were represented by 86 grid points. Bar elements were used to model the mast and the feed and solar panels, and rod elements for the hoop joints, hoop support, and surface shaping cables.

The total weight of the system is 2790 kg, of which the feed assembly is approximately 30%, the hoop and the mast 20%, and the solar panels and the spacecraft 50%. Since mass distribution affects modal frequencies, it is appropriate to point out that, based on subsequent study of a 122-m-diam LMSS[6] (land mobile satellite service) antenna, a much heavier (approximately 50%) weight concentration at the feed area is more realistic.

The finite element analysis revealed that the lowest mode is the first torsional mode, which has a frequency of 0.10 Hz. The next higher modes are the two orthogonal mast bending modes with frequencies of 0.43 Hz. The next two modes are the second and third mast torsion modes, followed by two orthogonal second mast and dish bending modes. Figure 2 shows the modal and mass properties. It is important to note that the antenna has relatively high bending stiffness and weak torsional stiffness. The high radial separation of the

hoop and the mast, the large hoop moment of inertia, and the small moment arm of the hoop cables at the mast make the mast very loosely coupled to the hoop so that the mast alone dominates the torsional modes.

III. The Attitude and Structural Control System

A. Equations of Motion

For small perturbations about the equilibrium, the dynamics of the system may be described by the finite element model. Let q be the 18-modal amplitude vector, Φ the 1236×18 eigenvector matrix, and f the vector of applied forces. The dynamic equations are, in component form,

$$\ddot{q}_k = \phi_k^T f, \qquad k=1,\ldots,6 \tag{1a}$$

$$\ddot{q}_k + 2\zeta_k\omega_k\dot{q}_k + \omega_k^2 q_k = \phi_k^T f, \qquad k=7,\ldots,18 \tag{1b}$$

where the modal frequencies ω_k may be obtained from Fig. 2 and the estimated values for the damping ratios ζ_k are 0.01 for $k=7,\ldots,10$ and 0.02 for $k=11,\ldots,18$.

Due to the existence of numerical sensitivity problems, the rigid modes were not used and Euler's equations were used instead to describe the rigid body motion. Referring to Fig. 2, let X, Y, Z be the body-fixed coordinates. Consider a nadir pointing configuration with the satellite moving in a circular synchronous orbit. The Euler's equations for the rigid-body rotation are

$$I_x\ddot{\phi} + 4\omega_0^2(I_y - I_z)\phi + \omega_0(I_y - I_x - I_z)\dot{\psi} = T_{dx} + T_{cx} \tag{2a}$$

$$I_y\ddot{\theta} + 3\omega_0^2(I_x - I_z)\theta = T_{dy} + T_{cy} \tag{2b}$$

$$I_z\ddot{\psi} + \omega_0^2(I_y - I_x)\psi + \omega_0(I_x - I_y + I_z)\dot{\phi} = T_{dz} + T_{cz} \tag{2c}$$

where I_x, I_y, I_z, ω_0, ϕ, θ, and ψ are the principal moments of inertia, the orbital rate, and the roll, pitch, and yaw angles, respectively. T_{dx}, T_{dy}, T_{dz}, T_{cx}, T_{cy}, and T_{cz} are the disturbance and control torques, respectively. Note that since the gravity gradient torques and the gyroscopic torques are already included in the left-hand side of Eq. (2), they are excluded from T_d. The angles ϕ, θ, ψ, and their derivatives in Eq. (2) are assumed to be small and they are related to inertial angular rates by the following approximate relations.

$$\omega_x = \dot{\phi} - \psi\omega_0 \qquad \omega_y = \dot{\theta} - \omega_0 \qquad \omega_z = \dot{\psi} + \phi\omega_0$$

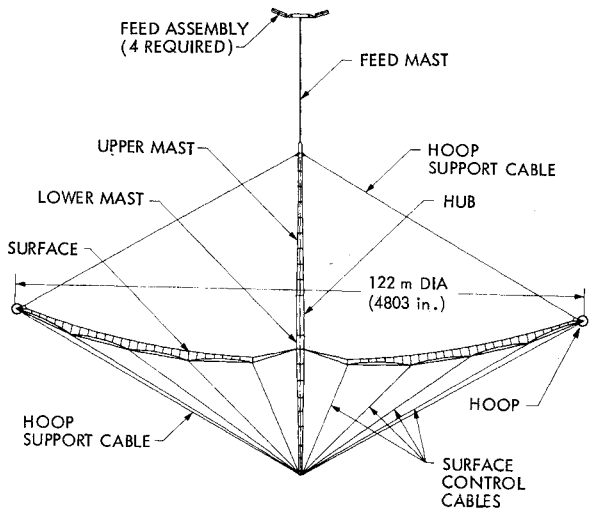

Fig. 1 Cross section of the 122-m-diam antenna.

B. Control Hardware Placement

The beam pointing accuracy is determined by the orientations of the feed and the dish and their relative motions. Sensor and actuator placements are dictated by the observability and controllability properties and the structural constraints. By examining the eigenvectors of the elastic modes at various potential locations, it can be seen that sensors and actuators placed at the feed assembly and the spacecraft bus can most effectively control the attitude and the important elastic modes. Figure 3 shows the two-site three-axis attitude and structural control system considered in this paper. Basic control devices are the inertial sensors and momentum wheels. Reflector shape control can be achieved with the addition of optical sensors such as SHAPES[4] and shape-cable actuators. Hoop motion can be controlled with a SHAPES sensor and thrusters on the hoop sections.

C. Controller Design

In the following, consider the three rigid-body modes and the seven low-frequency elastic modes. By close examination of the eigenvectors, the pitch bending modes (9 and 13) are separable from the roll bending modes (8 and 12) and the torsional modes (7, 10, and 11). Therefore, the pitch controller can be separately treated from the roll and yaw controller. The subscripts p and γ will be used to distinguish the two sets of controller parameters, respectively. However,

- MODAL FREQUENCIES

NO.	FREQ, HZ	DESCRIPTIONS
7	0.10	1ST MAST TORSION
8	0.43	1ST MAST ROLL BENDING
9	0.43	1ST MAST PITCH BENDING
10	0.58	2ND MAST TORSION
11	1.07	3RD MAST TORSION
12	1.83	2ND MAST/DISH ROLL BDG
13	1.90	2ND MAST/DISH PITCH BDG
14	3.20	DISH WARPING
15	3.28	DISH WARPING
16	3.36	DISH WARP MAST BENDING
17	3.37	DISH WARP MAST BENDING
18	4.43	DISH WARP MAST BENDING

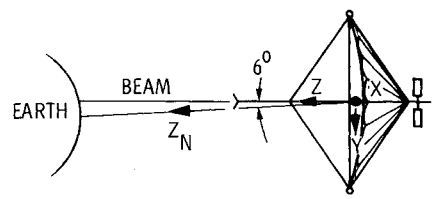

- 64 mD ANTENNA
- QUAD-APERTURE

- MASS PROPERTY
  - MASS: 2790 Kg
  - MOMENT OF INERTIA
    1.42×10^6 Kg-m^2
    1.42×10^6
    2.73×10^5
  - BALANCED CONFIGURATION

- MAX DISTURBANCE TORQUES
  - GRAVITY GRADIENT 1.89×10^{-3} Nm
  - GYROSCOPIC 6.30×10^{-4}
  - SOLAR PRESSURE 6.23×10^{-3}

Fig. 2 Structural properties for the 64-m-diam mesh deployable antenna.

when the context is clear, the subscripts will be dropped for clarity.

Pitch Controller Formulation

Consider the steady-state stochastic linear optimal output feedback regulator problem. For conciseness, only a minimum set of equations along with the assignment of variables will be given here without detailed explanations. (The p subscript is dropped here.) Referring to Fig. 4, let the state $x=(\theta,\ \dot{\theta};\ q_9,\dot{q}_9;\ q_{13},\dot{q}_{13})^T$; the measurement $z=(\theta_{pb},\dot{\theta}_{pb};\ \theta_{pf},\ \dot{\theta}_{pf})^T$, where b is the spacecraft bus and f the feed base; the plant disturbances $w=(T_{dyb},\ T_{dyf},\ F_{dxb},\ F_{dxf})^T$; the measurement noises $v=(v_{yab},\ v_{yrb},\ v_{yaf},\ v_{yrf})^T$, where a is the attitude and r the attitude rate; and the control torques $u=(T_{yb},\ T_{yf})^T$. The state and state estimator equations are

$$\dot{x}=Fx+Gu+\Gamma w \tag{3a}$$

$$z=Hx+v \tag{3b}$$

$$u=-K_{pc}\hat{x} \tag{3c}$$

$$\dot{\hat{x}}=F\hat{x}+Gu+K_{pe}(z-H\hat{x}) \tag{3d}$$

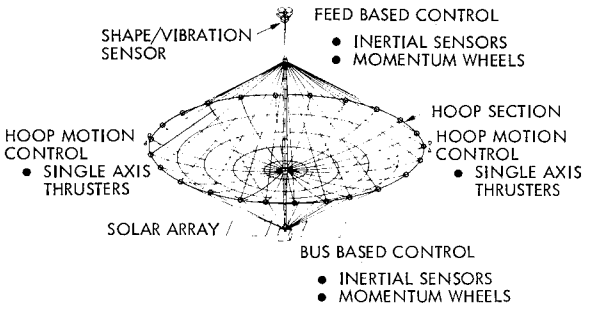

Fig. 3 Two-site control system.

The cost index to be minimized is

$$J_p=\frac{1}{2}E\left[\int_0^\infty (x^TA_px+u^TB_pu)\,dt\right] \tag{4}$$

The optimal control gains K_{pc} and the filter gains K_{pe} are, respectively,

$$K_{pc}=B_p^{-1}G^TS \tag{5a}$$

$$K_{pe}=PH^TR_P^{-1} \tag{5b}$$

where S and P satisfy the following algebraic equations, respectively:

$$SF+F^TS-SGB_p^{-1}G^TS+A_p \quad =0 \tag{6a}$$

$$FP+PF^T-PH^TR_P^{-1}HP+\Gamma Q_p\Gamma^T \quad =0 \tag{6b}$$

where A_p is the state weighting matrix, B_p the control weighting matrix, Q_p the spectral density matrix for the plant disturbances, and R_p the spectral density matrix for the measurement noises in the pitch axis. All of these matrices are to be constructed in the succeeding sections.

The F matrix is block diagonal and it can be constructed from Eqs. (1b) and (2b). G, H, and Γ can be obtained using the eigenvector data.

Roll and Yaw Controller Formulation

The system equations for the roll and yaw control are similar to those of Eqs. (3-6) with the subscript p replaced by γ. The variables x, z, u, w, and v are as follows:

$$x=(\phi,\dot{\phi};\psi,\dot{\psi};q_7,\dot{q}_7;q_8,\dot{q}_8;q_{10},\dot{q}_{10};q_{11},\dot{q}_{11};q_{12},\dot{q}_{12})^T$$

$$z=(\phi_{\gamma b},\dot{\phi}_{\gamma b};\psi_{\gamma b}\dot{\psi}_{\gamma b};\phi_{\gamma f}\dot{\phi}_{\gamma f};\psi_{\gamma f},\dot{\psi}_{\gamma f})^T$$

$$u=(T_{xb},T_{xf},T_{zb},T_{zf})^T$$

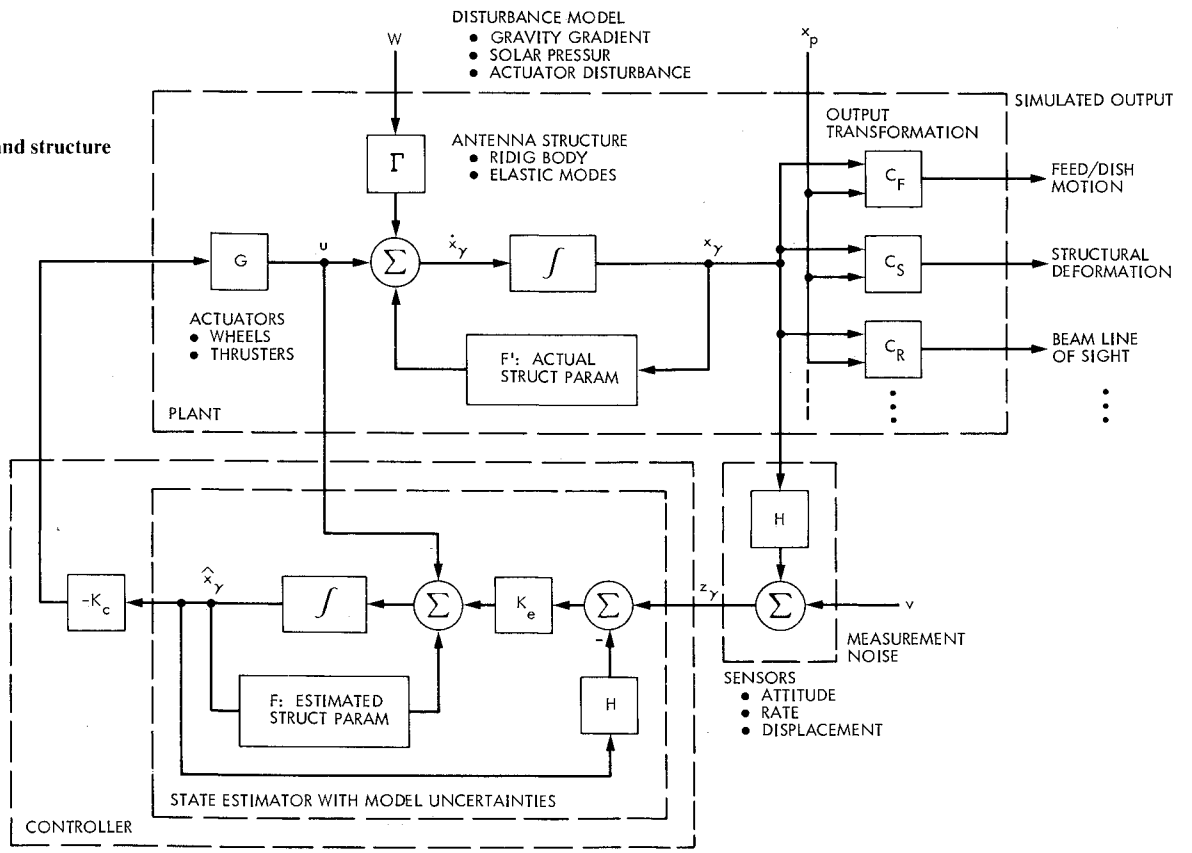

Fig. 4 Attitude and structure control system.

$$w=(T_{dxb},T_{dxf},T_{dzb},T_{dzf},F_{yb},F_{yf})^T$$

$$v=(v_{xab},v_{xrb};v_{zab}v_{zrb};v_{xaf},v_{xrf};v_{zaf},v_{zrf})^T$$

The state matrix is again block diagonal and can be obtained from Eqs. (1b), (2a), and (2c). Other matrices are defined similar to those in the pitch control case. The control system block diagram is shown in Fig. 4 with $F'=F$.

Before proceeding to the controller designs, the disturbances and the control hardware need to be characterized.

Characterization of Disturbances and Sizing of Control Hardware

The disturbances discussed here are limited to the gravity gradient and gyroscopic torques due to nonprincipal axis pointing, solar pressure torques, and torques caused by thruster firings for wheel dumping and stationkeeping.

Consider the LMSS antenna applications. With the current antenna design, the body z axis has to tilt 6 deg from nadir in order to provide the necessary communication coverage. A gravity gradient torque and gyroscopic torque of -2.52×10^{-3} N·m is created about the x axis. Since this torque is noncyclic, a periodic wheel dumping at the rate of 217.73 N·m·s for every 24 h is required. The solar pressure torques, however, are cyclic. With the availability of a detailed configuration for a 122-m-diam antenna, the solar pressure torques for the latter have been computed for arbitrary sun inclination and orbital position. Figure 5 shows these torques and the angular momentum. The solar pressure torques for the 64-m-diam antenna are obtained by scaling and consideration of the shift of the center of mass. Figure 6 shows the combined angular momentum due to solar pressure, gravity gradient, and gyroscopic torques for the 64-m-diam antenna.

Figures 6a and 6b show that the wheel capacity for the X and Y axes are about the same, assuming no dumping for the Y wheel and one dump per day for the X wheel. Using an empirical formula[5] with the weight w in pounds and the angular momentum H in foot-pounds-second,

$$w=7H^{0.4} \tag{7}$$

the weight for the four wheels (two for the X axis and two for the Y axis) will be 120 lb.

Consider two 0.1 lb Y thrusters, one at the feed base and one at the bus for X wheel dumping. These thrusters will produce 11.6 N·m of X torque, which is far more than the wheels can take. In order to maintain the antenna attitude to within ±0.02 deg per axis, the thrusters must be pulsed. The unloading may take 4 min if the thrusters are pulsed in 14 s on and 145 s off cycles.

Stationkeeping requires additional feed- and bus-based thrusters. Since the center of motion is located closer to the bus, if the feed-based thrusters are of the 0.1 lb size, the bus $\pm X$ and $\pm Y$ thrusters must be larger, or 0.2207 lb.

Hardware sizing allows for assessment of onboard disturbances. Assuming 10% disturbance level and 1 s correlation time, the power spectral density (PSD) for the disturbance forces are 9.68×10^{-4} and 4.82×10^{-3} N^2·s and that for the wheel torque disturbances is 0.02 $(N\cdot m)^2$·s with a 0.1 N·m disturbance level assumed. Using the subscripts SK for stationkeeping and WD for wheel dumping, the estimated power spectral density matrices are

$$Q_{pSK}=\text{Diag}(0.02,0.02;4.82\times10^{-3},9.68\times10^{-4}) \tag{8a}$$

$$Q_{pWD}=\text{Diag}(0.02,0.02) \tag{8b}$$

$$Q_{\gamma SK}=\text{Diag}(0.02,0.02,0.02,0.02,;4.82\times10^{-3},9.68\times10^{-4}) \tag{9a}$$

$$Q_{\gamma WD}=\text{Diag}(0.02,0.02,0.02,0.02;9.68\times10^{-4},\ 9.68\times10^{-4}) \tag{9b}$$

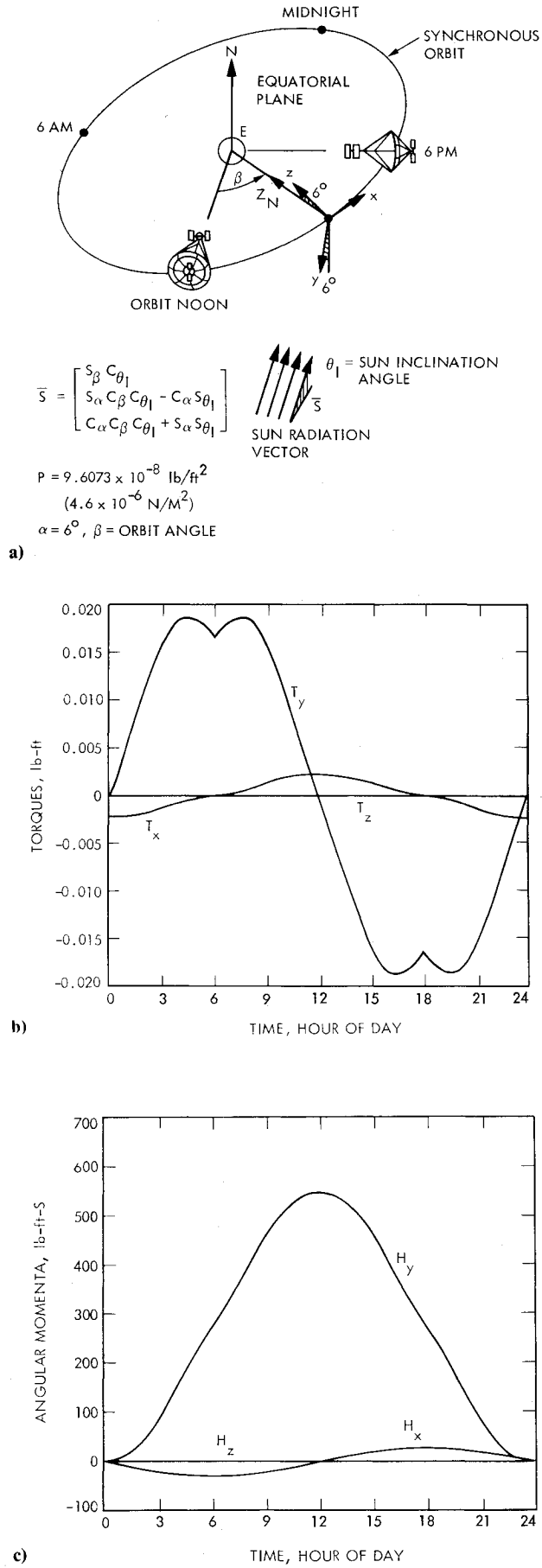

Fig. 5 Solar pressure torques for a 122-m-diam reflector quad-aperture antenna: a) orbital configuration; b) solar pressure torques with $\alpha=6$ deg and $\theta_I=0$ deg; and c) angular momenta for $\alpha=6$ deg and $\theta_I=0$ deg.

The sensor noise PSDs are estimated as follows. The attitude stability requirement for communications satellites is in the order of 0.04 deg overall, or 0.023 deg per axis. Assuming a 10% noise level and 0.1 s correlation time, the PSD for the attitude sensors will be 3.2×10^{-10} (rad)$^2\cdot$s. For the rate sensors, letting the measurement resolution be 1.75×10^{-4} rad/s with a correlation time of 0.05 s, the estimated PSD will be 3.06×10^{-9} (rad/s)$^2\cdot$s. With these estimates, the matrices R_p and R_γ are,

$$R_p=\text{Diag}(3.2\times10^{-10},3.06\times10^{-9},3.2\times10^{-10},3.06\times10^{-9}) \tag{10}$$

and

$$R_\gamma=\text{Diag}(3.2\times10^{-10},3.06\times10^{-9},\ldots,3.2\times10^{-10},3.06\times10^{-9}) \tag{11}$$

Construction of State Weighting Matrix

The selection of the state and control weighting matrices determines the control design. The state weighting matrix must reflect control objectives such as requirements on stability, surface, and pointing errors, etc. Consider pitch control. Let $A_p=\text{Diag}(a_1,a_2;a_3,a_4;a_5,a_6)$. The odd elements, in general, contribute to the stiffness of the closed-loop state and the even terms affect the damping.

The a_{2n+1} terms are determined by the weighted normalized mean square structural attitude angles, feed displacements, and dish deformations. More specifically, they may be expressed as

$$a_1=\frac{g_\theta}{(S_\theta)^2} \tag{12a}$$

$$a_3=\frac{g_F}{n_F(S_F)^2}\sum_{i_F}(\phi^2_{9xi}+\phi^2_{9yi}+\phi^2_{9zi}) + \frac{g_D}{n_D(S_D)^2}\sum_{i_D}(\phi^2_{9xi}+\phi^2_{9yi}+\phi^2_{9zi}) \tag{12b}$$

$$a_5=\frac{g_F}{n_F(S_F)^2}\sum_{i_F}(\phi^2_{13xi}+\phi^2_{13yi}+\phi^2_{13zi}) + \frac{g_D}{n_D(S_D)^2}\sum_{i_D}(\phi^2_{13xi}+\phi^2_{13yi}+\phi^2_{13zi}) \tag{12c}$$

where the subscripts F and D refer to feed and dish, respectively; n_D is the number of grid points on the dish, i_D means grid point i on the dish, ϕ_{9xi} is the translational mode shape for mode 9 at grid i; S_D is the specified rms surface displacement. Other parameters are similarly defined. The weighting factors g_θ, g_F, and g_D reflect the relative importance of the individual requirements. The values for the weighting factors were chosen to be 10, 20, and 5, respectively. This selection was guided by the feed and reflector optical properties. The construction of the roll and yaw state weighting matrix is similar.

D. Performance Evaluation Model

The control system performances that are of particular interest are the attitude and surface accuracy achievable in the projected disturbance environment, the relative stability, and the robustness of the controller in the presence of model parameter errors. These performance measures may be evaluated through computer simulations of the transient responses or the steady-state analysis of the statistical averages. The relative stability can be obtained from the closed-loop eigenvalues. The parameter error sensitivity problem will be discussed in the subsequent sections. In this subsection, we shall concentrate on the development of the evaluation models for the attitude errors, surface deformations, etc., using the state covariance matrix X.

Let X_{CP} and $X_{C\gamma}$ be the augmented state covariance matrices for pitch and roll and yaw control and estimation

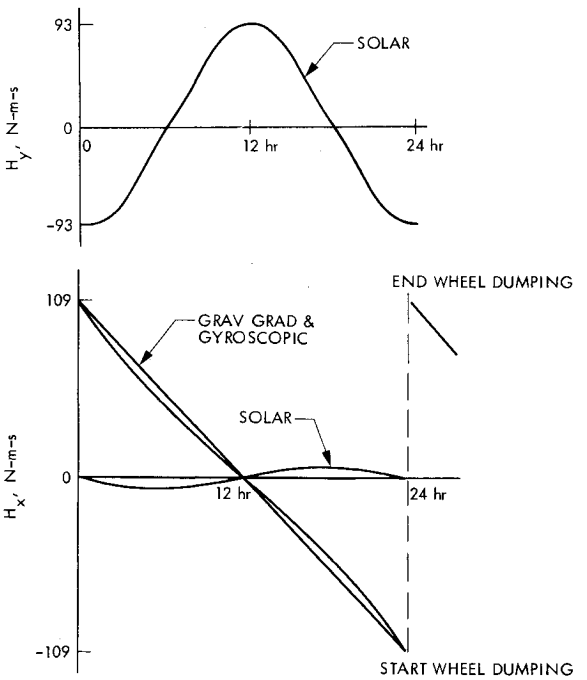

Fig. 6 Angular momentum accumulated over a 24 h period for the 64-m-diam antenna: a) Y axis angular momentum, and b) X axis angular momentum.

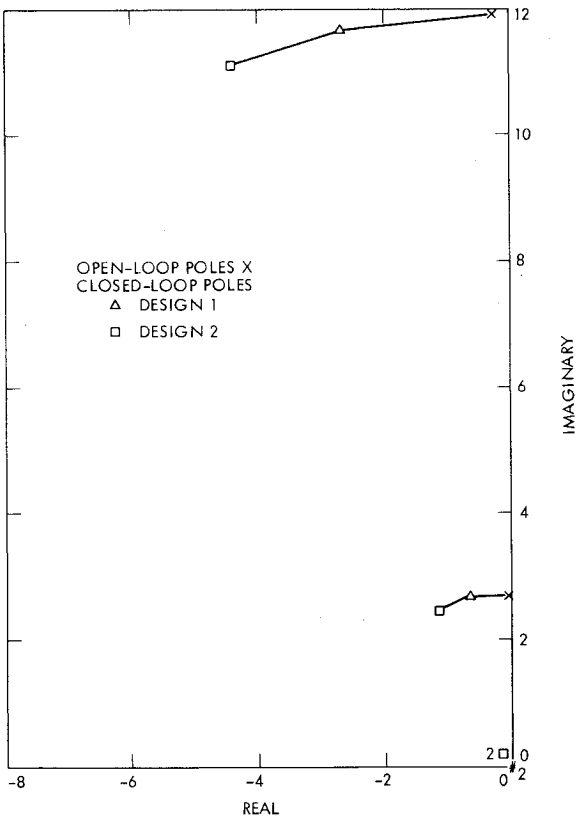

Fig. 7 Closed-loop control poles for two pitch controller designs.

respectively. The values for X_{CP} and $X_{C\gamma}$ may be obtained by solving the following matrix algebraic equations:

$$F_{CP}X_{CP}+X_{CP}F^T_{CP}+\Gamma_{CP}Q_{CP}\Gamma^T_{CP}=0 \tag{13}$$

$$F_{C\gamma}X_{C\gamma}+X_{C\gamma}F^T_{C\gamma}+\Gamma_{C\gamma}Q_{C\gamma}\Gamma^T_{C\gamma}=0 \tag{14}$$

where F_{CP}, $F_{C\gamma}$, Γ_{CP}, and $\Gamma_{C\gamma}$ are the state matrices and the disturbance influence matrices respectively for the

augmented closed-loop system defined in Eq. (19) with $F'=F$. Q_{CP} and $Q_{C\gamma}$ are the power spectral densities of w_{CP} and $w_{C\gamma}$, respectively, also defined in Eq. (19). The rms attitude error σ_A, the rms dish deformation σ_D, and the rms feed displaceemnt σ_F may be defined in terms of the covariance matrices as

$$\sigma_A = (X_\phi + X_\theta + X_\psi)^{1/2} \tag{15}$$

$$\sigma_D = \left[\frac{1}{n_D}\operatorname{tr}(\phi_{Dp}^T \phi_{Dp} X_{qp}) + \frac{1}{n_D}\operatorname{tr}(\phi_{D\gamma}^T \phi_{D\gamma} X_{q\gamma})\right]^{1/2} \tag{16}$$

$$\sigma_F = \left[\frac{1}{n_F}\operatorname{tr}(\phi_{Fp}^T \phi_{Fp} X_{qp}) + \frac{1}{n_F}\operatorname{tr}(\phi_{F\gamma}^T \phi_{F\gamma} X_{q\gamma})\right]^{1/2} \tag{17}$$

where X_ϕ, X_θ, X_ψ, X_{qp}, and $X_{q\gamma}$ are submatrices of X_{CP} and $X_{C\gamma}$, and ϕ_{Dp}, $\phi_{D\gamma}$, ϕ_{Fp}, and $\phi_{F\gamma}$ are submatrices of the eigenvector matrix Φ. For instance, X_{qp} and ϕ_{Dp} are

$$X_{qp} = \begin{bmatrix} E(q_9^2) & E(q_9 q_{13}) \\ E(q_9 q_{13}) & E(q_{13}^2) \end{bmatrix}$$

and

$$\phi_{Dp} = \begin{bmatrix} \phi_{9x15}\cdots\phi_{9x134} & \phi_{9y15}\cdots\phi_{9y134} & \phi_{9z15}\cdots\phi_{9z134} \\ \phi_{13x15}\cdots\phi_{13x134} & \phi_{13y15}\cdots\phi_{13y134} & \phi_{13z15}\cdots\phi_{13z134} \end{bmatrix}^T_{360x2}$$

and in Eqs. (16) and (17) $\operatorname{tr}(\cdot)$ is the trace of the matrix in the argument.

The rms control effort is also of interest and can be obtained from the control covariance matrices as follows:

$$U_p = K_{pc} X_p K_{pc}^T \tag{18a}$$

$$U_\gamma = K_{\gamma c} X_\gamma K_{\gamma c}^T \tag{18b}$$

$$U_{\text{rms}} = [\operatorname{tr}(U_p + U_\gamma)]^{1/2} \tag{18c}$$

where the covariance matrices X_p and X_γ are the submatrices of X_{Cp} and $X_{C\gamma}$.

The rms attitude error in Eq. (15) is the attitude of the entire structure or the rigid-body attitude. Therefore, it is not the beam pointing attitude. The actual beam pointing error is a function of the relative motions of the feed, dish, and dish surface deformation in addition to the structural attitude defined in Eq. (15).

The attitude errors at the feed and at the bus can be easily defined, however, in terms of the variables discussed in this section. Figure 4 shows the attitude and structural control system with the outputs defined here. The quantitative results are discussed in Sec. IV.

E. Model Parameter Error Problem

In Sec. III.C the control system has been defined with the assumption that the structural parameters were known. However, in reality large space system parameters cannot be accurately predicted on the ground. The result of this model error could seriously destabilize the system. Let F' be the actual state matrix and F be the modeled state matrix. Let e be the estimator error, $\hat{x}-x$. The system may be represented as

$$\begin{bmatrix} \dot{x} \\ \dot{e} \end{bmatrix} = \begin{bmatrix} F'-GK_c & -GK_c \\ F-F' & F-K_eH \end{bmatrix} \begin{bmatrix} x \\ e \end{bmatrix} + \begin{bmatrix} \Gamma & 0 \\ -\Gamma & K_e \end{bmatrix} \begin{bmatrix} w \\ v \end{bmatrix} \tag{19a}$$

where the following notations have been used in the foregoing discussions

$$x_C = \begin{bmatrix} x \\ e \end{bmatrix} \qquad F_C = \begin{bmatrix} F'-GK_c & -GK_c \\ F-F' & F-K_eH \end{bmatrix} \tag{19b}$$

and

$$\Gamma_C = \begin{bmatrix} \Gamma & 0 \\ -\Gamma & K_e \end{bmatrix} \qquad w_C = \begin{bmatrix} w \\ v \end{bmatrix} \tag{19c}$$

In the absence of model errors, i.e., $F'=F$, the eigenvalues of the closed-loop system are those determined by $\det(F-GK_c)$ and $\det(F-K_eH)$. For this type of controller, the system is asymptotically stable. However, when $F' \neq F$, stability cannot be guaranteed and destabilization can occur if F' is sufficiently different from F as demonstrated in the next section. Note in Eq. (19) the gain matrices are designed based on the modeled system parameters.

IV. Numerical Results

A. Design Experiments

For the linear system (F,G,Γ,H), it is well known that the numerical values of the A and B matrices determine the control gains and Q and R determine the filter gains. The odd diagonal terms of A can be computed using Eq. (12). For the even terms, the rigid-body part can be normalized to the square of a fraction (say 1/10) of the lowest modal frequency associated with that axis and then multiplied by a weighting factor; the elastic terms may be obtained by multiplying the corresponding odd terms by weighting factors. The B matrix may be obtained by normalizing the nominal actuation forces or torques and then weighting them. Q and R are fixed by disturbance and noise properties; however, for the purpose of obtaining desirable filter properties, their values may be varied and the actual values should be restored for evaluation. Other techniques, such as destabilization, may be used to

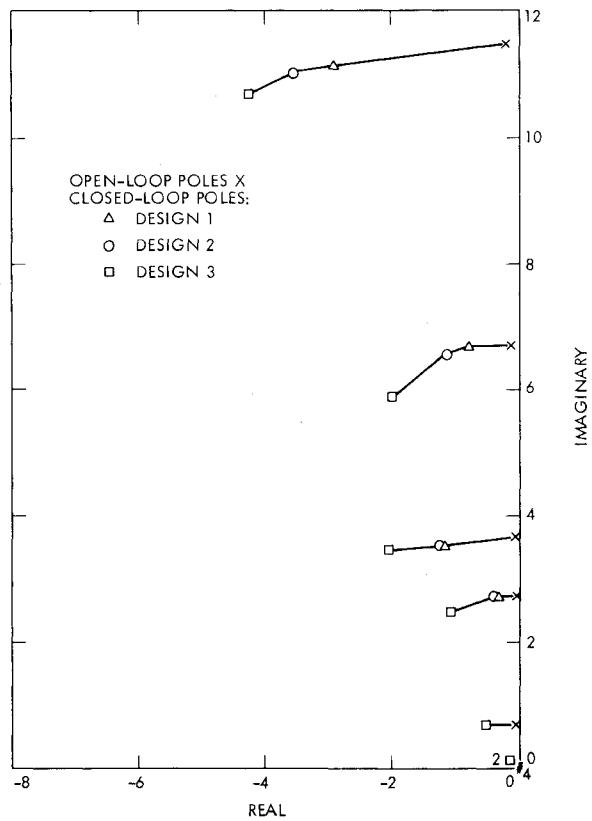

Fig. 8 Closed-loop control poles for three roll and yaw controller designs.

obtain desirable closed-loop pole placement for both the control and estimation.

Many trial runs may be required to reach a good design. Figure 7 shows two pitch control designs and Fig. 8 three roll and yaw designs. The various cases were obtained by varying the even diagonal weights of the A matrix while holding the odd terms at constant value. As illustrated in these figures, by increasing the values of the even elements, the damping for the corresponding elastic modes increases. By reducing these values to zero, the controller will have essentially no effect on the elastic modes and the closed-loop poles will move to the open-loop poles.

B. Control Performance

Designs discussed in the preceding subsection have yielded reasonable performance. Figure 9 shows the feed and the bus pointing errors with parameter error varying 70-130%. The controller becomes unstable if the parameter errors exceed these boundaries. Figure 10 shows a similar result for the feed displacement. In all cases when the actual frequencies increased the performance has improved somewhat. This is because the structure becomes stiffer as the frequency increases.

One important question that needs to be addressed here is how much a two-site control is better than a one-site control system. Figure 11 demonstrates that the two-site control system is more robust than either of the two one-site control systems.

Further comparisons for the three control concepts are in Fig. 12 where the identifications of critical modal parameters are made. The bending modes are less critical to all but the single-site feed control system. The torsional modes are critical to all the systems and they set the stability limits for both the single-site bus control and the two-site control systems.

In addition to the stability margin properties, the results of Figs. 9-11 also show that, to the extent studied here, the antenna as modeled can be controlled to meet the near-term communications satellites (e.g., LMSS[6]) performance requirements.

Finally, considering the model errors, with current structural modeling technology, including the computer tools such as NASTRAN programs, modal parameters for the first few low-frequency modes of a large space structure are expected to be modeled to an accuracy of within 5-15%, of 15-30% for the next few modes, and of 30-50% or worse for higher modes. Since large space structures have not been flown before, the true modeling capability and model uncertainties can be determined only through flight experiments and in-flight system identification. Because of this high model uncertainty, the authors felt that it would be adequate to expose the error sensitivity problem by allowing the parameter errors to vary over the $\pm 30\%$ range.

V. Discussion

The design approach of this paper is based on the principle that by stiffening the structure, dampening the vibrations, and pointing the structure and the structural components, one has in effect pointed the rf beams to the desired orientations. Alternatively, one may construct the cost functional in such a way that rf-beam-related quantities (such as field strength at selected points) are optimized. Although much of the rf-based control design idea has yet to be explored before its effectiveness can be critically assessed, initial work in this area by the Jet Propulsion Laboratory is beginning to show promising results. However, one must realize that the control of a large operational space structural system involves the incorporation of a multitude of objectives encompassing both the structural integrity and stability, as well as rf performance. A viable solution to this problem is a balanced integrated structural and rf design.

In any event, regardless of the design approaches discussed here, the controller is instructed to steer the mechanical structure to form a line of sight that will "ideally" aim the rf beam to its target; this is quite different from directly steering the beam to its target. In the context of large space antennae, it is very difficult to state in precise terms where the beam is pointing. Deformations of reflector surface (static and dynamic) and displacements of the feed and dish (angular and translational) will cause field pattern changes, uneven side lobes, defocus, and cross polarization. It will be a formidable

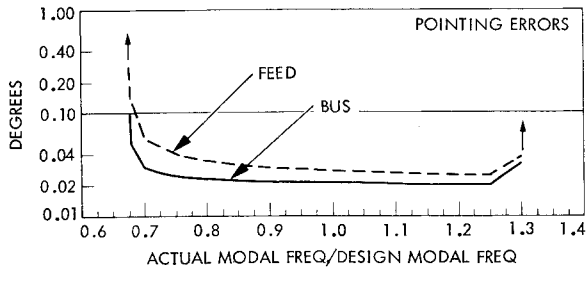

Fig. 9 RMS pointing accuracy.

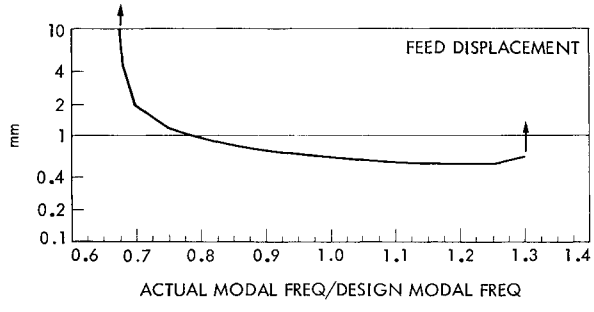

Fig. 10 RMS feed displacement.

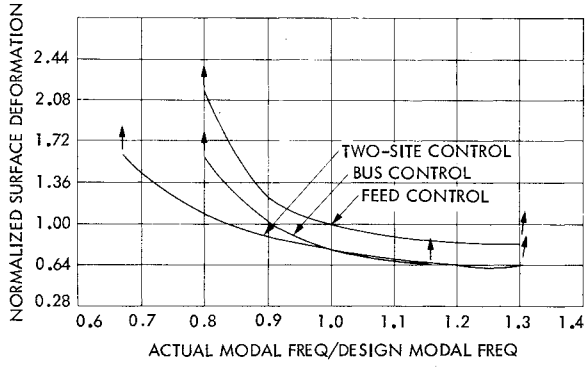

Fig. 11 Stability regions for three control systems.

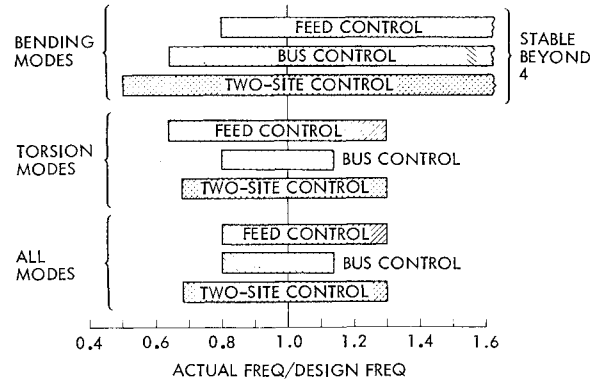

Fig. 12 Stability regions subject to parameter errors.

job to find an equivalent beam based on the stochastic structural deformations of the antenna. However, when the shape or mechanical errors are small, say a small fraction of the wavelength, then one may infer that the structural line of sight determines the beam direction. In this paper, the structural model does not possess enough resolution to permit precise rf beam definition and, hence, it is outside the realm of in-depth discussion.

VI. Conclusions

The principal antenna control system objective is to point the radio frequency beams to the desired destinations within prescribed stability and pointing accuracy while maintaining overall system alignment and figure to meet required performance characteristics. To achieve this objective on a flexible structure of 50-120 m represents a substantial challenge especially when margins are needed to accommodate dynamic model uncertainties. Specific conclusions are summarized as follows:

1) Structural uncertainties and model errors can cause serious performance deterioration and can even destabilize the controllers.

2) For the specific antenna configuration on hand, the large hoop and long mast and the lack of stiffness between the two substructures result in low structural frequencies. Performance can be improved if this design is strengthened.

3) The two-site control system is more robust than either single-site control system. The two-site control concept has resulted in reasonable hardware requirements when applied to a communications mission.

4) Every new technology requires extensive testing and evaluation before it can be applied to space systems. Large flexible space structures have never been flown. Broad-based ground test and flight experiments will be necessary to reduce uncertainties and to establish a high level of confidence and provide guidance for improvement.

Acknowledgments

The research described in this paper was carried out by the Jet Propulsion Laboratory, California Institute of Technology, under contract with the National Aeronautics and Space Administration.

References

[1]Russell, R.A., Campbell, T.G., and Freeland, R.E., "A Technology Development Program for Large Space Antennas," Paper IAF-80 A33, 31st International Astronautical Congress of the International Astronautical Federation, Tokyo, Sept. 21-28, 1980.

[2]Tankerslay, B.D., "Maypole (Hoop/Column) Deployable Reflector Concept Development for 30 to 100 Meter Antenna," Conference on Advanced Technology for Future Space Systems, Hampton, Va., May 8-10, 1979.

[3]"LSST Hoop/Column Antenna Development Program, Phase I, Final Program Review," Harris Corp., Melbourne, Fla., Rept. NAS1-15763, Vol. 1, Oct. 1980.

[4]McLauchlan, J.M., Goss, W.C., and Tubbs, E.F., "SHAPES: A Spatial High-Accuracy, Position-Encoding Sensor for Space Systems Control Applications," Paper AAS 32-032, AAS Annual Rocky Mountain Guidance and Control Conference, Keystone, Colo., Jan. 30-Feb. 3, 1980.

[5]Dougherty, H.J. et al., "Attitude Stabilization of Synchronous Communications Satellites Employing Narrow-Beam Antennas," *Journal of Spacecraft and Rockets*, Vol. 8, Aug. 1971, pp. 834-841.

[6]Naderi, Firouz, ed., "Land Mobile Satellite Service (LMSS): A Conceptual System Design of the Critical Technologies," Jet Propulsion Laboratory, Pasadena, Calif., JPL Pub. 82-19, Feb. 15, 1982.